Article

Investigating the Shear Characteristics of Geomembrane–Sand Interfaces Under Freezing Conditions

Dun Chen [1,2], Guoyu Li [1,2], Pengfei He [3,4,*], Hang Zhang [2], Jie Sheng [2] and Miao Wang [5]

[1] State Key Laboratory of Frozen Soil Engineering, Northwest Institute of Eco-Environment and Resources, 320 Donggangxilu Rd., Lanzhou 730000, China; chendun@lzb.ac.cn (D.C.); guoyuli@lzb.ac.cn (G.L.)
[2] Electric Power Research Institute, State Grid Heilongjiang Electric Power Company Limited, Harbin 150030, China; zhanghang@hepri.hl.sgcc.com.cn (H.Z.); sj881230@163.com (J.S.)
[3] School of Civil Engineering, Lanzhou University of Technology, 287 Langongping Rd., Lanzhou 730000, China
[4] Lanzhou GongDa Engineering Testing Technology Co., Ltd., 194 Xijinxilu Rd., Lanzhou 730050, China
[5] Heilongjiang Provincial Hydraulic Research Institute, Harbin 150050, China; jyllwm1990@126.com
* Correspondence: hepf17@163.com; Tel.: +86-1391-9281-468

Abstract: This study experimentally investigates the effects of freezing conditions on the shear characteristics of geomembrane–soil interfaces, employing a temperature-controlled direct shear apparatus. The findings reveal significant variations in shear stress–shear displacement patterns at the soil–geomembrane interface under different thermal conditions. At positive temperatures, the interface manifests strain hardening behavior, whereas at negative temperatures, it transitions from weak softening at low normal stress to strong strain softening at high normal stress. The shear displacement–normal displacement curves under varying temperature and normal stress conditions demonstrate dilatant behavior, with initial increases in normal displacement followed by a decrease as temperature drops. Notably, the interface friction angle is markedly higher at negative temperatures compared to positive, undergoing an initial increase, a period of stable development, and a subsequent rise with further temperature reduction. The average shear strength ratio at the interface is observed to be as low as 0.58 at 20 °C, approaches unity between −2 °C and −6 °C, and exhibits a significant increase at −10 °C. These findings are helpful for the application of geomembranes in frozen soil engineering.

Keywords: soil–geosynthetic interaction; shear strength; strength ratio; frozen soil; friction angle

1. Introduction

Geosynthetics were integral to the field of civil engineering due to their exceptional impermeability, economic viability, favorable elasticity, and ease of construction [1]. Amidst the challenges posed by global warming and increasingly stringent carbon emission constraints in engineering construction, optimizing the long-term performance of geotechnical structures and mitigating carbon emissions through the application of geosynthetics has emerged as a critical research avenue. Among the diverse family of geosynthetics, geomembranes are particularly noted for their role as barriers against liquid or gaseous flow, effectively curtailing the migration of harmful substances or water through soil. Their utility is evident in a spectrum of engineering applications, including reservoirs, dams, landfills, reinforced soil slopes, and canals [2,3].

In their roles as barriers or reinforcements in landfill systems, embankments, footings, and reinforced embankments, etc., geomembranes are frequently in direct contact with soil. Given the significant disparity in strength and stiffness between these two materials, the

geomembrane–soil interface is prone to slippage under the influence of gravity or external loads. Consequently, the shear strength at the geomembrane–soil interface is a pivotal parameter for ensuring the stability of structures that incorporate geomembranes. Accurate assessment of the shear resistance at this interface is essential during the design and construction phases to prevent structural failure that may arise from interface slippage [4,5].

Direct shear tests, pullout tests, and slope stability tests are commonly employed to investigate the shear characteristics at the geomembrane–soil interface [6,7]. The direct shear test, favored for its straightforward apparatus and ease of controlling experimental conditions, allows for the direct measurement of the shear stress–strain relationship and the determination of interface shear strength between soil and geomembrane [8]. Consequently, it has garnered widespread application in research. Empirical evidence suggests that the surface characteristics of the geomembrane, including roughness and texture, as well as the properties and conditions of the soil, such as particle size, shape, and density, significantly influence the shear strength at the interface [9,10].

Fleming et al. [11] delved into the shear strength of the geomembrane–soil interface under unsaturated conditions, uncovering that the effective stress–shear strength relationship of the interface could be anticipated by employing the principles of unsaturated soil mechanics, particularly at low normal stress levels [11]. Markou and Evangelou [12] conducted direct shear tests to scrutinize the shear resistance characteristics of the soil–geomembrane interface, discovering a pronounced dependence of shear resistance parameters on soil particle shape and geomembrane surface characteristics [12]. Araujo et al. [13] meticulously examined the impact of geomembrane surface roughness parameters on the shear strength of various interfaces through a comprehensive suite of inclined plane tests coupled with microscopic surface roughness analyses. Their findings revealed a robust correlation between the mean height profile element and the core material volume parameters with interfacial shear strength. Consequently, they introduced the interfacial roughness factor as a metric to estimate the interfacial friction between geomembranes and geotextiles, predicated on material properties [13]. Khan and Latha [14,15] quantitatively characterized the particle shape and size and the surface roughness of the geomembrane, identifying a significant influence of particle shape on the interface strength and its formation process. Chao et al. [16], capitalizing on data from 623 laboratory interface direct shear experiments, developed a machine learning model to predict the peak shear strength of the clay–geomembrane interface, highlighting that atmospheric pressure is the most influential factor on peak shear strength, surpassed only by geomembrane roughness. Sergio Luiz da Costa Junior [17] performed direct shear tests on textured geomembranes with varying bump heights against two distinct soil types, observing no significant impact of bump height on interface parameters, indicating the necessity to assess additional textural properties. Feng and Wang [18] conducted a series of direct interface shear tests on three distinct geomembranes against soil, employing a novel machine learning model that effectively forecasted the peak friction angle of the interface.

Furthermore, the interfacial behavior between geomembranes and soil masses is significantly influenced by varying hydrothermal and mechanical conditions, as well as by the test environments in direct shear tests [19,20]. Over 25% of the global land area is classified as permafrost regions. During temperature oscillations between positive and negative values, the freezing of water into ice within the soil substantially affects the soil's physical and mechanical properties [21]. Generally, soil strength tends to increase with decreasing freezing temperatures [22]. However, during the interaction between frozen soil and structures, the frost heave deformation of the soil and the structural deformation is often asynchronous, leading to a propensity for interface slippage. The shear properties of the interface between frozen soil and traditional construction materials, such as concrete,

metal, and wood, have been extensively studied. Studies indicate that the interfacial shear strength increases with decreasing temperature due to changes in the cemented ice content and temperature within the soil and at the interface, with material properties exerting a significant influence [23,24]. Geosynthetics, as a novel construction material with broad application prospects, are increasingly utilized in permafrost regions. The shear properties of the interface between geosynthetics and frozen soil under diverse freezing conditions and the impact of freeze-thaw cycles have garnered considerable research interest [25]. As a flexible construction material, the shear properties and the soil particle movement characteristics (e.g., sliding, adhesion, friction, interlocking) of geosynthetics at the interface with frozen soil markedly differ from those of traditional building materials [20].

While existing research has yielded valuable insights into the shear characteristics of the geomembrane–soil interface, there remain challenges and limitations in understanding the mechanical behavior of this interface under diverse freezing conditions. Although geosynthetics are derived from similar raw materials, such as high-density polyethylene (HDPE) and polyvinyl chloride (PVC), the weaving methods employed during their production can significantly vary. Consequently, the shear behavior of the geomembrane–soil interface under different freezing conditions remains poorly understood.

Therefore, there is a pressing need for further investigation into the response of the geomembrane–soil interface shear behavior to varying freezing temperatures. This paper presents the design of a geomembrane–soil interface test system capable of controlling freezing temperatures, based on the direct shear test method. The study analyzes the evolution of shear stress–shear displacement relationships, the variation of interfacial shear strength, and the change in strength ratio under different freezing temperatures and normal pressures. The findings of this research aim to provide a deeper understanding of the interface shear characteristics, thereby enabling engineers to more accurately assess and predict interfacial shear strength during the design of geomembrane-related structures. This, in turn, will contribute to enhancing the safety and economic efficiency of such structural designs.

2. Materials and Methods

2.1. Soil

The test soil was sourced from Lanzhou City, China, a region characterized by seasonal freezing with an average maximum freezing depth of 1 m. Employing the Unified Soil Classification System (USCS) as outlined in ASTM D2487 [26], the soil was classified as sandy (SP) with a coefficient of curvature (CC) of 1.36 and a coefficient of uniformity (Cu) of 5.45. During the soil treatment process, particles larger than 2 mm in size were meticulously removed. The particle gradation is shown in Table 1. The soil's optimal moisture content was determined to be 9%, and its maximum dry density was found to be 1.8 g/cm^3. The fundamental mechanical properties of the sand were ascertained through direct shear testing, with the stress–displacement curves and the corresponding strength variation laws depicted in Figure 1. Figure 1a illustrates that the shear stress–shear displacement curves of the sand under various normal stress conditions exhibit strain-softening behavior. Figure 1b demonstrates that both the peak shear strength and the corresponding peak shear displacement increase with the augmentation of normal stress, with the internal friction angle of the sand determined to be 43.4°.

Table 1. The particle gradation of testing soil.

Particle size (mm)	<0.075	0.075~0.1	0.1~0.25	0.25~0.5	0.5~1	1~2
Percentage (%)	4.0	4.0	13.4	31.0	27.9	19.7
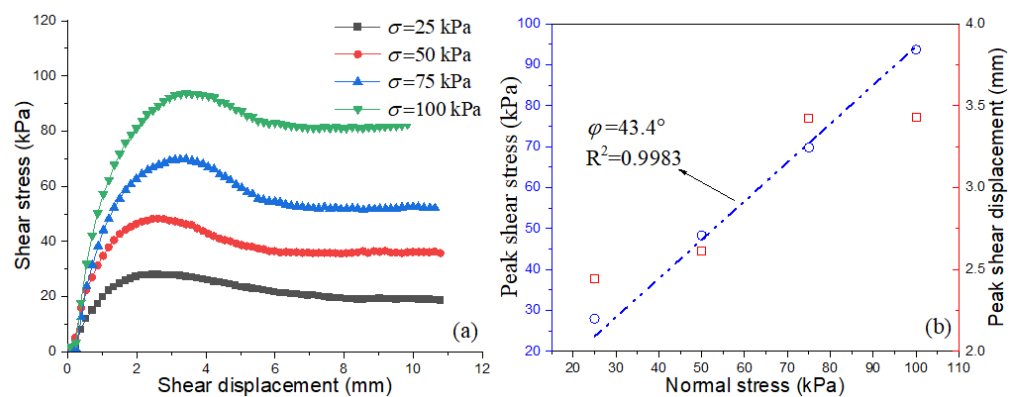
Figure 1. Direct shear test results of sand. (**a**) Shear stress–shear displacement curves under varying normal stress. (**b**) Peak shear stress and peak shear displacement with varying normal stress.

2.2. Geomembrane

The geomembranes utilized in this study are high-density polyethylene (HDPE) with a smooth and flat surface, as depicted in Figure 2. These geomembranes have a thickness of 5 mm and a density of approximately 0.95 g/cm^3. Following the standard prescribed test methods outlined in ASTM D4885 [27], the mechanical properties of the geomembranes are detailed in Table 2.
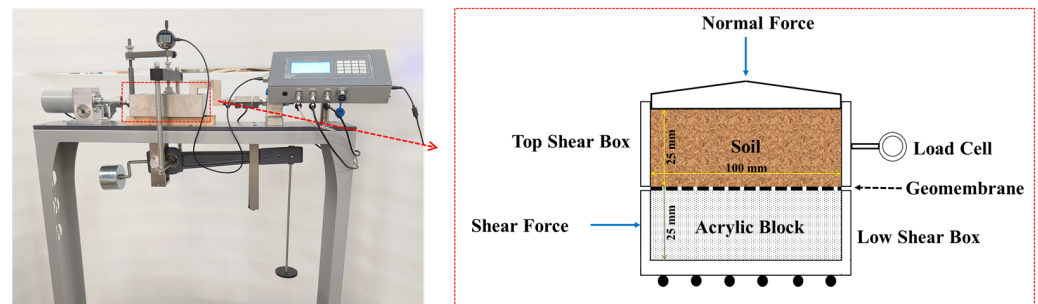

Figure 2. Photo of geomembranes.

Table 2. Mechanical properties of geosynthetics.

Maximum lateral tensile strength	15.975	kN/m
Maximum portrait tensile strength	15.987	kN/m
Maximum lateral elongation	50.24	%
Maximum portrait elongation	42.43	%
CBR bursting strength	2.788	kN
Lateral tear strength	0.450	kN
Portrait tear strength	0.454	kN

2.3. Test Process

The direct shear test device is a ubiquitous tool in the investigation of soil and interfacial mechanical properties [20,23,24,28]. Figure 3 illustrates the schematic diagram of the direct shear apparatus employed in this study. The apparatus consists of two shear boxes, each measuring 25 mm in height, 100 mm in length, and 100 mm in width. Normal

pressure is applied to the upper box via a lever system, while the lower box is actuated to move horizontally by a motor. The horizontal displacement of the lower box, the horizontal load on the upper box, and the normal displacement of the upper box are all automatically recorded by a computer system. To ensure the precision of temperature control during testing, the direct shear instrument is housed within a temperature-controlled chamber, with the thermostat maintaining a control accuracy of $\pm 0.2\,^{\circ}\text{C}$.

Figure 3. Photo and schematic diagram of the interface shear test apparatus.

In the fabrication process of the soil–geomembrane samples, the geomembrane is affixed to an acrylic plate using high-viscosity adhesive. The combined height of the acrylic plate and geomembrane is approximately 25 mm, allowing for alignment with the interface of the upper and lower boxes of the direct shear instrument. Subsequently, the adhesive acrylic plate and geomembrane are placed into a sample mold, and soil is compacted layer by layer above the geomembrane. Ultimately, the prepared soil–geomembrane interface shear samples are sealed in plastic film and incubated at a constant temperature for 24 h to ensure uniform temperature distribution.

The shear rate employed in the tests was set at 0.8 mm/min, with test normal pressures of 25 kPa, 50 kPa, 75 kPa, and 100 kPa. The test temperatures were controlled at 20 °C, -2 °C, -4 °C, -6 °C, and -10 °C, respectively. The testing procedure adhered to the guidelines of the standard test method as outlined in ASTM D3080 [28].

2.4. Interfacial Shear Parameters

The Mohr–Coulomb failure criterion, with its clear physical significance, is extensively applied to characterize the shear strength of soils and soil–structure interfaces [29–33].

$$\tau = c + \sigma_{\text{n}}\tan\varphi \tag{1}$$

where τ is shear strength, c is cohesion, σ_{n} is normal stress, and φ is internal friction angle.

If we extend this criterion to fit the shear strength of the interface between the soil mass and a structure, such as a geomembrane, the equation can be adapted to account for interface-specific parameters. The interface adhesion is denoted as c_i and the interface friction angle as φ_i. The adapted Mohr–Coulomb equation for the interface shear strength (τ_i) then becomes the following:

$$\tau_i = c_i + \sigma_{\text{n}}\tan\varphi_i \tag{2}$$

This equation allows for the calculation of interface-specific shear strength parameters, which are crucial for understanding and predicting the behavior of soil–structure interfaces under various loading conditions. By fitting experimental data to this equation, researchers can extract the values of c_i and φ_i that best describe the shear resistance at the soil–structure interface.

Indeed, the interfacial shear strength between soil and geosynthetic materials such as geomembranes and geotextiles is often lower than the shear strength of the soil itself, which can lead to increased potential for slippage at the interface. This ratio, which reflects the relative shear resistance and thus the stability of the interface, is a critical parameter in geotechnical engineering. It can be quantified using the following formula:

$$\text{Interface Strength Ratio} = \frac{\tau_{interface}}{\tau_{soil}} \tag{3}$$

where $\tau_{interface}$ is the shear strength at the soil–geosynthetic interface and τ_{soil} is the shear strength of the soil mass itself.

This ratio indicates how the interface shear strength compares to the shear strength of the soil, providing insight into the potential for interface failure. A lower ratio suggests a higher risk of slippage and a potential area for geotechnical concern. Engineers can use this ratio to assess the stability of soil–geosynthetic systems and to design appropriate measures to enhance interfacial adhesion, thereby improving the overall stability of geotechnical structures.

3. Results and Analysis

Figure 4 illustrates the response of the soil–geomembrane interface under varying normal pressures at a temperature of 20 °C. Figure 4a depicts the shear stress–shear displacement curves, which exhibit a strain hardening trend across the different normal pressures. Initially, the shear stress increases rapidly with shear displacement, followed by a gradual deceleration in the rate of increase until a stable state is reached. In this stable state, the shear strength is observed to increase with normal pressure. This is attributed to the granular nature of the soil, where particle friction plays a predominant role in the interaction at the soil–geomembrane interface [2,31,33]. As normal pressure increases, the contact between soil particles and the geomembrane surface becomes more intimate, necessitating greater energy expenditure during shearing to achieve relative displacement between the two. Figure 4b presents the relationship between normal and horizontal displacements, indicating dilatant behavior at the interface under different normal pressures. Before reaching the peak shear displacement, normal displacement increases with shear displacement; post-peak, the displacement stabilizes. Notably, normal displacement decreases with increasing normal stress, with the maximum normal displacement ranging from 0.32 mm at 25 kPa to 0.15 mm at 100 kPa.

Figure 4c delineates the variation law of the interface peak shear strength and the strength ratio under various normal pressures. It is observed that the interface friction angle is 28.5°, which constitutes merely 65.7% of the soil's inherent friction angle. The intensity ratio, under different normal pressures, exhibits minimal variation, fluctuating between 0.54 and 0.62. This significant reduction in interface strength is identified as a pivotal factor influencing the composite structure of geosynthetic materials [32].

Figure 5 presents the response of the soil–geomembrane interface under varying normal pressures at −2 °C. Post-freezing, the unfrozen water content within the soil decreases with the reduction in temperature, typically experiencing a rapid decline phase before stabilizing at an equilibrium value. During freezing, the formation of ice crystals increases, leading to the development of ice cementation within the soil. The strength of this ice cementation, and consequently the frozen soil, increases with decreasing temperature [20]. Figure 5a indicates that the shear stress–shear displacement curve at the −2 °C interface transitions from a strain hardening behavior at 20 °C to a strain softening behavior, with the softening effect being more pronounced under higher normal pressures. This is attributed to the brittle nature of the cemented ice in frozen soil, which imparts a brittle characteristic

to the interface's mechanical response [21,22]. Initially, the interface undergoes elastic deformation. As shear displacement increases, the bonds between the interface soil, cemented ice, and geomembrane are progressively broken, leading to the emergence of brittle fractures in the cemented ice. Additionally, since ice is a frictionless material, it contributes minimally to interface strength post-failure of the cemented ice. These factors collectively result in a rapid decrease in interfacial shear stress post-peak strength, manifesting as strain softening behavior. Figure 5b illustrates the relationship between normal and shear displacements at −2 °C, revealing dilatant deformation at the interface under different normal pressures. Comparing the normal displacement at 20 °C as shown in Figure 4b, it is observed that normal displacement increases at −2 °C. This increase is attributed to the formation of larger soil–ice aggregates post-freezing, which, during shearing, roll and cause greater changes in normal displacement [34–37]. Figure 5c depicts the changes in peak shear strength and strength ratio at the interface under various normal pressures. The interface friction angle is found to be 44.9 °, which is 103% of the soil's inherent friction angle. This significant increase in interface friction angle compared to 20 °C is due to the formation of larger soil and ice particle aggregates post-freezing, which, when moved on the geomembrane surface, enhance the interface friction angle. The interfacial strength ratio varies from 0.91 to 1.25, indicating an increase in interfacial shear strength under the influence of cemented ice, thereby augmenting the strength relative to conditions at higher temperatures.

Figure 6 presents the response of the soil–geomembrane interface at −4 °C under various normal pressures. As depicted in Figure 6a, the shear stress–shear displacement curve exhibits strain hardening at 25 kPa, while at 50 kPa to 100 kPa, the curve demonstrates strain softening, with the softening phenomenon intensifying with increasing normal pressure. Figure 6b illustrates the relationship between normal displacement and shear displacement, indicating dilatant deformation at the interface under different normal pressures. With the augmentation of normal pressure, the normal displacement at the interface gradually diminishes, attributed to the restrictive effect of higher normal pressure on particle rolling and tumbling. Compared with Figure 5b, it is observed that the stability value of normal displacement at the interface at −4 °C remains largely unchanged from that at −2 °C, suggesting that the cemented ice between −2 °C and −4 °C exerts minimal influence on the volume or movement process of the soil particle–ice particle aggregate at the interface. Figure 6c displays the variations in peak shear strength and strength ratio at the interface under different normal pressures. The interface friction angle is found to be 43.8 °, which is 101% of the soil's friction angle, a similarity to the conditions at −2 °C. The interfacial strength ratio fluctuates between 0.82 and 1.09, suggesting that while the interfacial shear strength increases under the influence of cemented ice, resulting in higher strength compared to the relatively melting state, the change is marginal compared to the conditions at −2 °C.

Figure 7 illustrates the response of the soil–geomembrane interface under various normal pressures at −6 °C. As observed in Figure 7a, the shear stress–shear displacement curve exhibits weak softening at 25 kPa and 50 kPa and strong softening at 75 kPa and 100 kPa. Notably, at 75 kPa and 100 kPa, the shear stress rapidly decreases after reaching peak intensity and then undergoes a gradual increase to the residual stage. This phenomenon is attributed to the further decrease in temperature, which leads to an increase in the content of cemented ice at the interface. The increased cemented ice enhances the interfacial shear strength, and the brittle fracture becomes more pronounced when the stress reaches peak strength [5,24]. Figure 7b depicts the relationship between normal displacement and shear displacement, indicating dilatant deformation at the interface under different normal pressures, with a gradual decrease in normal displacement as normal pressure increases.

However, compared to the normal displacement at 2 °C (Figure 5b) to −4 °C (Figure 6b), it is evident that the normal displacement at −6 °C decreases significantly. As the temperature decreases, the content of cemented ice in the soil increases, enhancing the soil's strength and integrity. A multitude of soil particle–ice particle aggregates do not exhibit movement in geoengineering; instead, the tumbling and rolling of relatively smaller aggregates or soil particles and the sliding of the entire soil mass are observed [38]. Figure 7c presents the variation law of interface peak shear strength and strength ratio under different normal pressures. The interface friction angle is found to be 44.9 °, which is 103% of the soil's friction angle and similar to that at −2 °C and −4 °C. The interfacial strength ratio ranges between 0.91 and 1.18, suggesting that the interfacial shear strength increases under the influence of cemented ice, resulting in higher strength compared to the relatively melting state, but the change is minimal compared to conditions at −2 °C and −4 °C.
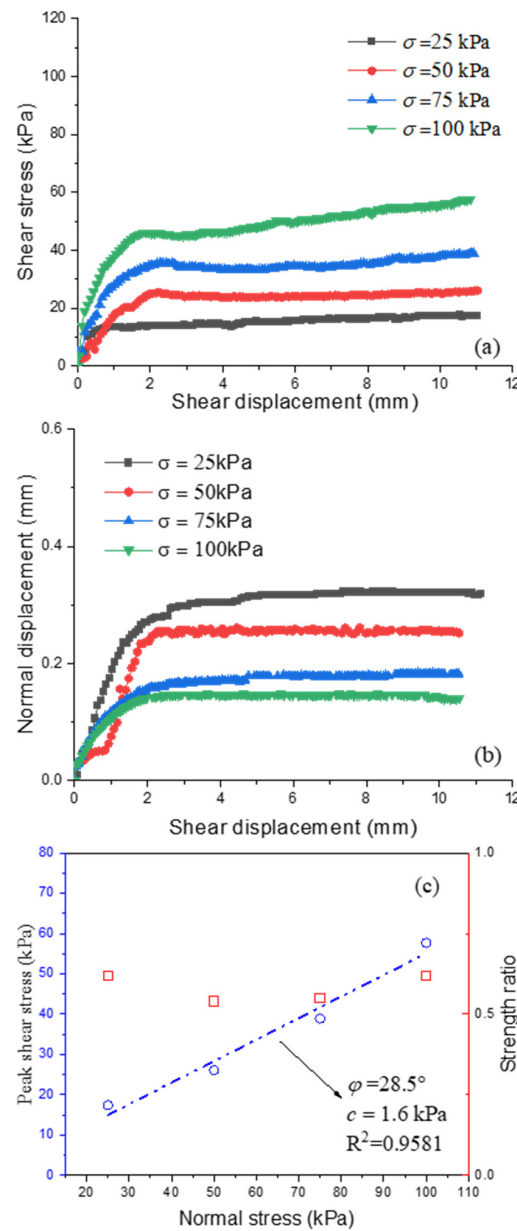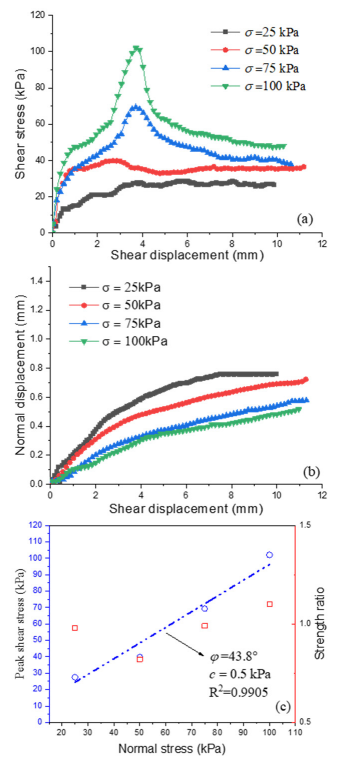

Figure 4. Interfacial shear response at 20 °C. (**a**) Shear stress–shear displacement curves under varying normal stress. (**b**) Normal displacement–shear displacement curves under varying normal stress. (**c**) Peak shear stress and strength ratio with varying normal stress.
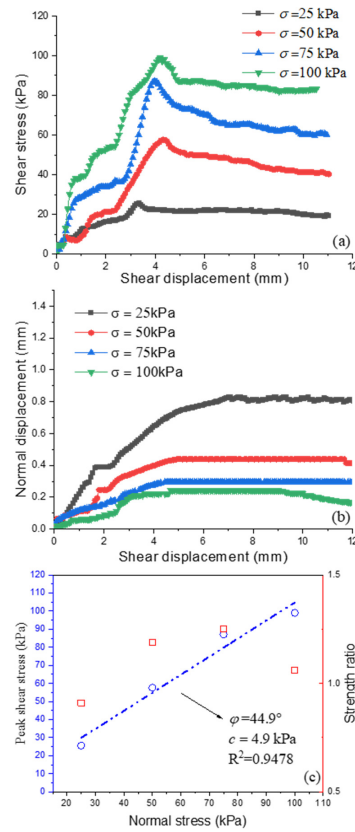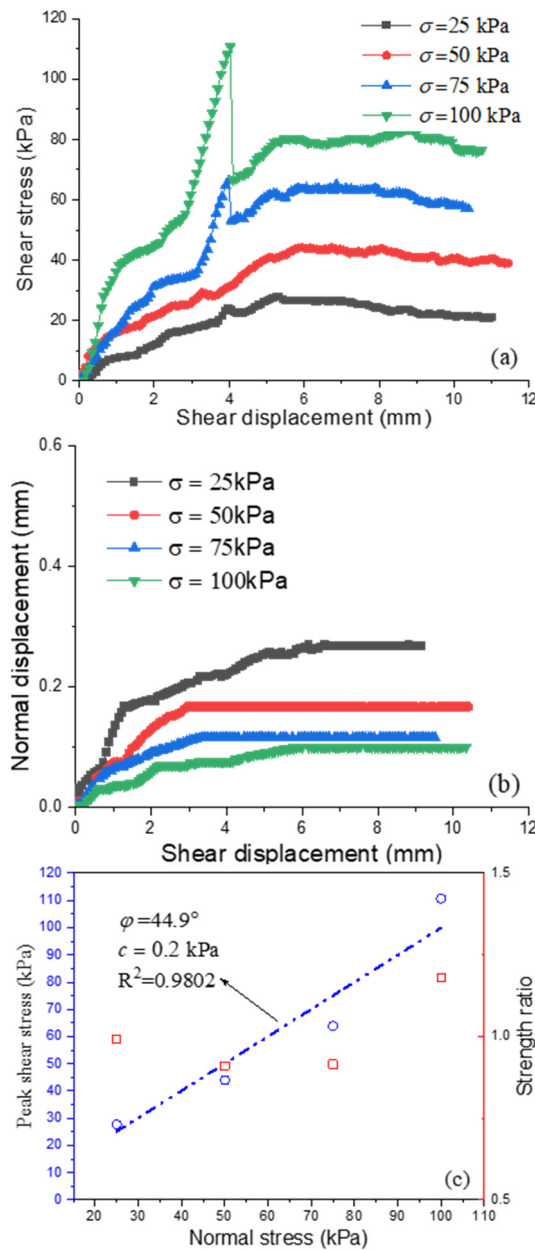
Figure 5. Interfacial shear response at −2 °C. (**a**) Shear stress–shear displacement curves under varying normal stress. (**b**) Normal displacement–shear displacement curves under varying normal stress. (**c**) Peak shear stress and strength ratio with varying normal stress.
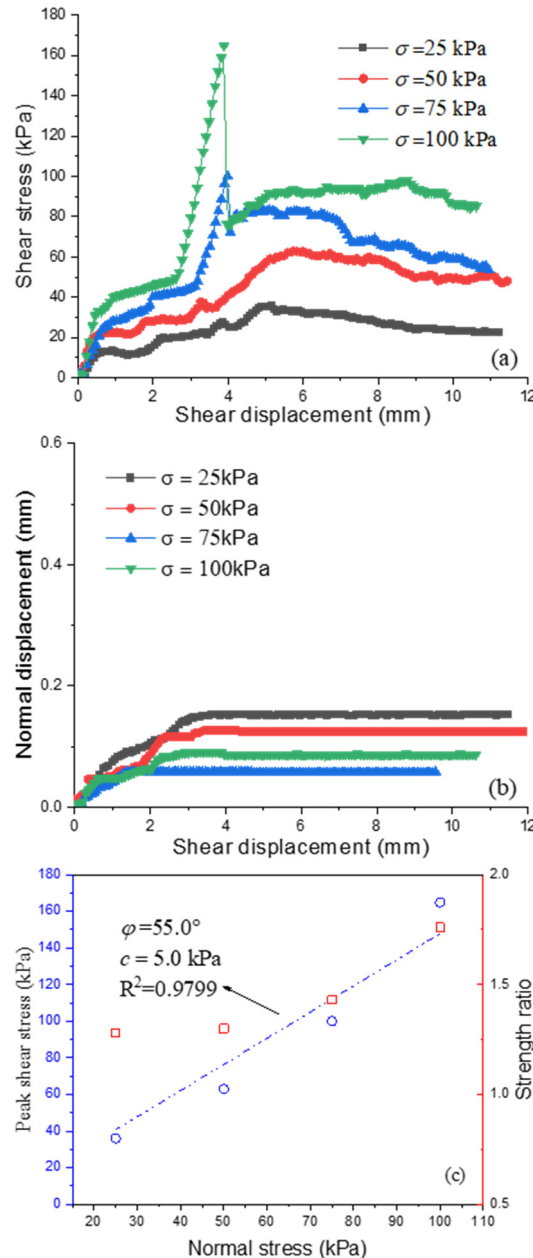

Figure 6. Interfacial shear response at −4 °C. (**a**) Shear stress–shear displacement curves under varying normal stress. (**b**) Normal displacement–shear displacement curves under varying normal stress. (**c**) Peak shear stress and strength ratio with varying normal stress.

Figure 7. Interfacial shear response at −6 °C. (**a**) Shear stress–shear displacement curves under varying normal stress. (**b**) Normal displacement–shear displacement curves under varying normal stress. (**c**) Peak shear stress and strength ratio with varying normal stress.

Figure 8 depicts the response of the soil–geomembrane interface under various normal pressures at −10 °C. As evident from Figure 8a, the peak shear strength of the interface experiences a significant increase, with the peak shear strength at 100 kPa being 49% higher than that observed at −6 °C. This enhancement is attributed to the substantial increase in ice content within the soil and the corresponding augmentation of the contribution of cemented ice to the interface shear strength. Notably, at 75 kPa and 100 kPa, there is a pronounced brittle fracture behavior. Figure 8b illustrates the relationship between normal displacement and shear displacement, indicating dilatant deformation at the interface under different normal pressures, with a gradual decrease in normal displacement as normal pressure increases. Comparing the normal displacement at −6 °C (Figure 7b), it is observed that the normal displacement at −10 °C is further reduced. Since the majority of the water in the soil has frozen into ice at −10 °C, the integrity of the soil mass is further strengthened. The interaction between the soil mass and the geomembrane

during interfacial shear is predominantly the sliding of the entire soil mass, resulting in minimal normal displacement during the shearing process [37]. Figure 8c presents the variation law of peak interfacial shear strength and strength ratio under different normal pressures. The interface friction angle is found to be 55.0 °, which is 127% of the soil's friction angle, showing a further increase compared to −6 °C. The interfacial strength ratio ranges between 1.29 and 1.76, indicating a further increase in interfacial shear strength under the influence of cemented ice.

Figure 8. Interfacial shear response at −10 °C. (**a**) Shear stress–shear displacement curves under varying normal stress. (**b**) Normal displacement–shear displacement curves under varying normal stress. (**c**) Peak shear stress and strength ratio with varying normal stress.

Figure 9 delineates the temperature-dependent variation of the interface friction angle and the average strength ratio. Figure 9a indicates that at 20 °C, the interface friction angle is significantly lower than that of the soil itself, highlighting the critical role of the soil–geomembrane interface in structural design considerations. As the temperature declines, the interface friction angle exhibits a pronounced increase, a result of the enhanced

contribution of cemented ice to both soil strength and the strength of the soil–geomembrane bond [19,20]. In freezing, the ice content in the soil gradually increases as the temperature decreases. The adhesion strength between the soil and the structure will also increase with the increase of the ice content at the interface [38]. Within the temperature range of −2 °C to −6 °C, the interface friction angle surpasses the soil's intrinsic friction angle, and at −10 °C, this angle increases dramatically. Figure 9b demonstrates that the average strength ratio at 20 °C is a concerningly low 0.58, which poses a significant risk for structures that incorporate geomembranes. Even with a design safety factor of 2, this ratio is alarmingly close to the threshold of ultimate strength. With the reduction in temperature, the strength ratio gradually ascends, approaching 1 between −2 °C and −6 °C, indicating that the interface strength at these temperatures is nearly equivalent to the soil's strength. However, this does not mean that the safety of the structure is enhanced. The potential for frost heave in soil upon negative temperatures still poses a risk of interface instability [39–41]. At −10 °C, the average strength ratio increases considerably, thereby augmenting the structural stability in comparison to higher temperatures.
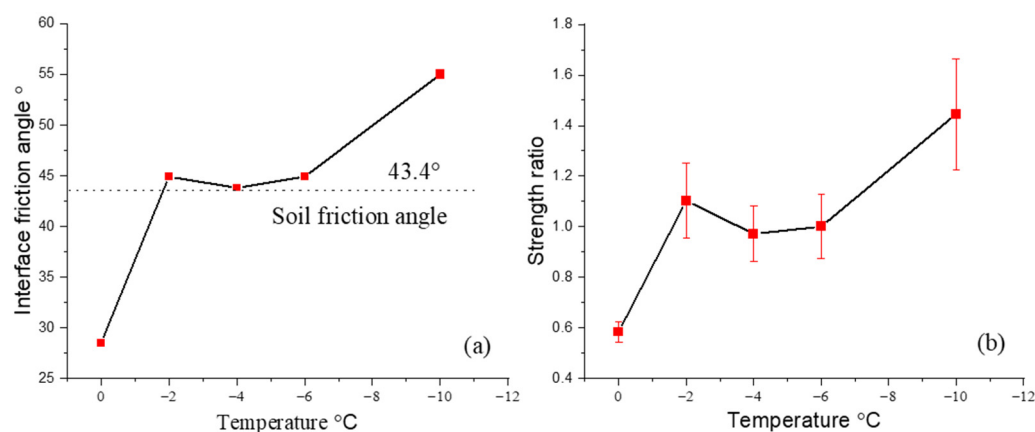
Figure 9. Changes of interfacial shear strength parameters at different temperatures. (**a**) Interface friction angle with temperature. (**b**) Strength ratio with temperature.

4. Conclusions

This study examines the shear behavior of the soil–geomembrane interface under varying temperature conditions and normal pressures using a temperature-controlled direct shear instrument. The analysis of the shear stress–shear displacement curves, shear displacement–normal displacement curves, interface friction angles, and strength ratios under different test conditions yields the following conclusions:

(1) The shear stress–shear displacement curve of the soil–geomembrane interface exhibits strain hardening characteristics at positive temperatures. Conversely, at negative temperatures, the curve displays weak softening at low normal pressures and strong softening at high normal stresses.

(2) Under diverse temperatures and normal stress conditions, the shear displacement–normal displacement curves of the interface manifest dilatant behavior. At positive temperatures, normal displacement is minimal due to the tumbling and sliding of relatively small soil particles on the geomembrane surface. However, as the temperature decreases, ice cementation leads to an increase in the aggregate volume of soil particles and cemented ice particles, resulting in increased normal displacement. Upon further temperature reduction, the overall strength of the soil is significantly enhanced after a substantial amount of water has frozen, and numerous soil grain-cemented ice particles are frozen as a whole, unable to roll on the geomembrane surface, thus reducing the corresponding normal displacement.

(3) The interface friction angle at negative temperatures is markedly higher than at positive temperatures. The interface friction angle initially increases, then stabilizes, and subsequently increases again with further temperature reduction. The average strength ratio of the interface is a concerningly low 0.58 at 20 °C, posing a significant risk for geomembrane-related composite structures. Even with a structural safety factor of 2, this ratio is alarmingly close to the ultimate strength threshold. The ratio approaches 1 between −2 °C and −6 °C and increases significantly at −10 °C. Due to varying degrees of frost heave in soil after the temperature drops to negative values, the interface remains susceptible to slippage.

In this paper, the shear characteristics of the interface between sand and geomembrane under different temperature conditions are explored only by direct shear test. In engineering systems such as canals and landfills, when the system enters the frozen state, the interfacial shear strength increases, and the system will face frost heave at the same time, but the direct shear test cannot measure the frost heave process, which needs to be studied in future work by physical model experiment.

Author Contributions: Conceptualization, P.H.; methodology, D.C. and P.H.; formal analysis, G.L. and P.H.; investigation, D.C.; resources, H.Z.; data curation, P.H. and J.S.; writing—original draft preparation, D.C.; writing—review and editing, P.H.; visualization, G.L. and M.W.; supervision, P.H.; project administration, G.L.; funding acquisition, G.L. All authors have read and agreed to the published version of the manuscript.

Data Availability Statement: The data used to support the findings of this study are included in the article.

References

1. Lin, H.; Gong, X.; Zeng, Y.; Zhou, C. Experimental study on the effect of temperature on HDPE geomembrane/geotextile interface shear characteristics. *Geotext. Geomembr.* **2024**, *52*, 396–407. [CrossRef]
2. Khan, R.; Latha, G.M. Multi-scale behaviour of sand-geosynthetic interactions considering particle size effects. *Geotext. Geomembr.* **2025**, *53*, 169–187. [CrossRef]
3. Xu, Y.; Yan, G.; Williams, D.J.; Serati, M.; Scheuermann, A.; Vangsness, T. Experimental and numerical studies of a strip footing on geosynthetic-reinforced sand. *Int. J. Phys. Model. Geotech.* **2020**, *20*, 267–280. [CrossRef]
4. Gayathri, V.L.; Vangla, P.; Dey, S. A versatile apparatus for assessing the shear behaviour of geotechnical interfaces coupled with imaging and acoustic capabilities. *Acta Geotech.* **2024**, *19*, 6217–6237. [CrossRef]
5. He, P.; Hou, G.; Cao, H.; Yue, F. The influence of geosynthetic properties on their shear behaviors at the interface with frozen soil. *Geotext. Geomembr.* **2025**, *53*, 497–509. [CrossRef]
6. Li, L.; Fall, M.; Fang, K. Shear behavior at interface between compacted clay liner–geomembrane under freeze-thaw cycles. *Cold Reg. Sci. Tech.* **2020**, *172*, 103006. [CrossRef]
7. Lakkimsetti, B.; Latha, G.M. Morphological insights into the liquefaction and post-liquefaction response of sands with geotextile inclusions using drained constant volume simple shear tests. *Geotext. Geomembr.* **2023**, *51*, 144–164. [CrossRef]
8. Hamidi, A.; Garousi, A.H. Grain size effect on the anisotropic shear behavior of sand–textured geomembrane interface. *Proc. Inst. Civ. Eng. -Ground Improv.* **2024**, *177*, 310–323. [CrossRef]
9. Punetha, P.; Mohanty, P.; Samanta, M. Microstructural investigation on mechanical behavior of soil-geosynthetic interface in direct shear test. *Geotext. Geomembr.* **2017**, *45*, 197–210. [CrossRef]
10. Lashkari, A.; Jamali, V. Global and local sand–geosynthetic interface behaviour. *Géotechnique* **2021**, *71*, 346–367. [CrossRef]

11. Fleming, I.R.; Sharma, J.S.; Jogi, M.B. Shear strength of geomembrane–soil interface under unsaturated conditions. *Geotexti. Geomembr.* **2006**, *24*, 274–284. [CrossRef]

12. Markou, I.N.; Evangelou, E.D. Shear resistance characteristics of soil–geomembrane interfaces. *Int. J. Geosynth. Ground Eng.* **2018**, *4*, 29. [CrossRef]

13. Araújo, G.L.S.; Sánchez, N.P.; Palmeira, E.M.; de Almeida, M.D.G.G. Influence of micro and macroroughness of geomembrane surfaces on soil-geomembrane and geotextile-geomembrane interface strength. *Geotext. Geomembr.* **2022**, *50*, 751–763. [CrossRef]

14. Khan, R.; Latha, G.M. Integrated digital image analyses for understanding the particle shape effects on sand–geomembrane interface shear. *Int. J. Geosynth. Groun.* **2023**, *9*, 81. [CrossRef]

15. Khan, R.; Latha, G.M. Multi-scale understanding of sand-geosynthetic interface shear response through Micro-CT and shear band analysis. *Geotext. Geomembr.* **2023**, *51*, 437–453. [CrossRef]

16. Chao, Z.; Shi, D.; Fowmes, G.; Xu, X.; Yue, W.; Cui, P.; Yang, C. Artificial intelligence algorithms for predicting peak shear strength of clayey soil-geomembrane interfaces and experimental validation. *Geotext. Geomembr.* **2023**, *51*, 179–198. [CrossRef]

17. da Costa Junior, S.L.; Lodi, P.C. Assessment of the interface shear strength between HDPE geomembrane and tropical soil by the direct shear test. *Contrib. Las Cienc. Soc.* **2023**, *16*, 9902–9915. [CrossRef]

18. Feng, Y.; Wang, D. Shear behaviors and peak friction angle predictions of three critical geomembrane–soil interfaces. *Acta Geotech.* **2024**, *19*, 3139–3160. [CrossRef]

19. Karademir, T.; Frost, J.D. Apparatus for geosynthetic interface testing and evaluation under elevated temperature conditions. *J. Test. Eval.* **2013**, *41*, 313–323. [CrossRef]

20. He, P.; Cao, H.; Dong, J.; Hou, G.; Mu, Y.; Zhang, J. Experimental study on the effect of freeze-thaw cycles on the shear characteristics of frozen soil-composite geotextile interface. Case Studies. *Therm. Eng.* **2024**, *54*, 104011.

21. Tang, L.; Sun, S.; Zheng, J.; Qiu, P.; Guo, T. Thermal conductivity changing mechanism of frozen soil-rock mixture and a prediction model. *Int. J. Heat Mass Transf.* **2023**, *216*, 124529. [CrossRef]

22. Qiu, P.; Tang, L.; Zheng, J.; Wang, W.; Li, Y.; Li, G.; Duan, X. Experimental investigations on the shear strength and creep properties of soil-rock mixture under freeze-thaw cycles. *Cold Reg. Sci. Tech.* **2024**, *217*, 104037. [CrossRef]

23. Shi, S.; Zhang, F.; Feng, D.; Xu, X. Experimental investigation on shear characteristics of ice–frozen clay interface. *Cold Reg. Sci. Tech.* **2020**, *176*, 103090. [CrossRef]

24. Pan, R.; Yang, P.; Yang, Z. Experimental study on the shear behavior of frozen cemented sand-structure interface. *Cold Reg. Sci. Tech.* **2022**, *197*, 103516. [CrossRef]

25. Meng, Y.; Xu, C.; Yang, Y.; Du, C.; Jia, B.; Zhao, C. Study on the mechanism of freeze-thaw cycles on the shear strength of geogrid-sand interface. *Cold Reg. Sci. Tech.* **2024**, *225*, 104275. [CrossRef]

26. *ASTM D2487*; Standard practice for Classification of Soils for Engineering Purposes (Unified Soil Classification System). American Society for Testing and Materials (ASTM): West Conshohocken, PA, USA, 2000.

27. *ASTM D4885-01*; Standard Test Method for Determining Performance Strength of Geomembranes by the Wide Strip Tensile Method. ASTM International: West Conshohocken, PA, USA, 2001.

28. Hassanikhah, A.; Miller, G.A.; Hatami, K. Laboratory investigation of unsaturated clayey soil-geomembrane interface behavior. *Geosynth. Int.* **2020**, *27*, 379–393. [CrossRef]

29. *ASTM D3080/D3080M-11*; Standard Test Method for Direct Shear Test of Soils under Consolidated Drained Conditions. ASTM International: West Conshohocken, PA, USA, 2011.

30. Hu, L.; Pu, J. Testing and modeling of soil-structure interface. *J. Geotech. Geoenviron. Eng.* **2004**, *130*, 851–860. [CrossRef]

31. Vangla, P.; Gali, M.L. Shear behavior of sand-smooth geomembrane interfaces through micro-topographical analysis. *Geotext. Geomembr.* **2016**, *44*, 592–603. [CrossRef]

32. Oggeri, C.; Ronco, C.; Vinai, R. Validation of numerical D.E.M. modelling of geogrid reinforced embankments for rockfall protection. *Geoingeg. Ambient. Mineraria* **2021**, *58*, 36–45.

33. Xu, Y.; Williams, D.J.; Serati, M. Measurement of shear strength and interface parameters by multi-stage large-scale direct/interface shear and pull-out tests. *Meas. Sci. Technol.* **2018**, *29*, 085601. [CrossRef]

34. Yavari, N.; Tang, A.M.; Pereira, J.M.; Hassen, G. Effect of temperature on the shear strength of soils and the soil–structure interface. *Can. Geotech. J.* **2016**, *53*, 1186–1194. [CrossRef]

35. Yin, K.; Fauchille, A.L.; Di Filippo, E.; Kotronis, P.; Sciarra, G. A review of sand–clay mixture and soil–structure interface direct shear test. *Geotechnics* **2021**, *1*, 260–306. [CrossRef]

36. Chen, W.B.; Zhou, W.H.; Yin, Z.Y. Recent Development on Macro–Micro Mechanism of Soil-Structure Interface Shearing Through DEM. *Arch. Comput. Methods Eng.* **2023**, *30*, 1843–1862. [CrossRef]

37. Junior, S.L.D.C.; Aparicio-Ardila, M.A.; Palomino, C.F.; Lins da Silva, J. Analysis of Textured Geomembrane–Soil Interface Strength to Mining Applications. *Int. J. Geosynth. Groun.* **2023**, *9*, 3. [CrossRef]

38. Wan, X.; Zhou, H.; Zhou, F.; Zhu, J.; Shahab, K.M. Mesoscopic shear evolution characteristics of frozen soil-concrete interface. *Cold Reg. Sci. Tech.* **2025**, *229*, 104342. [CrossRef]

39. Shi, Y.; Zhang, L.; Mu, Y.; Ma, W.; Kong, X.; Yang, C. Dynamic characteristics of soil pore structure and water-heat variations during freeze-thaw process. *Eng. Geol.* **2024**, *343*, 107785. [CrossRef]
40. Zhao, Y.; Zhang, M.; Gao, J. Research progress of constitutive models of frozen soils: A review. *Cold Reg. Sci. Tech.* **2023**, *206*, 103720. [CrossRef]
41. Jiang, H.; Zhang, M.; Wang, Z.; Gong, J.; Sun, X. Theoretical analysis of the mechanical response of a lined canal induced by soil frost heave behavior based on improved foundation beam models. *Cold Reg. Sci. Tech.* **2024**, *225*, 104252. [CrossRef]